Stability Analysis of MHD Stagnation-point Flow towards a Permeable Stretching/Shrinking Sheet in a Nanofluid with Chemical Reactions Effect

(Analisis Kestabilan Aliran Titik Genangan MHD terhadap Permukaan Telap Meregang/Mengecut dalam Nanobendalir dengan Kesan Tindak Balas Kimia)

FATINNABILA KAMAL, KHAIRY ZAIMI, ANUAR ISHAK* & IOAN POP

ABSTRACT

The magnetohydrodynamic (MHD) stagnation-point flow of a nanofluid towards a permeable stretching/shrinking sheet with chemical reaction effect is investigated. The governing nonlinear partial differential equations are transformed into a system of nonlinear ordinary differential equations using a similarity transformation which are then solved numerically using the boundary value problem solver, bvp4c built in Matlab software. The numerical results are obtained for the skin friction coefficient, local Nusselt number, local Sherwood number as well as the velocity, temperature and concentration profiles for some values of the governing parameters, namely suction/injection parameter and chemical reaction parameter. Dual solutions are found to exist for a certain range of the stretching/shrinking parameter. A stability analysis is performed to determine which solutions are stable and physically reliable. It is found that the first solutions are stable and the second solutions are unstable.

Keywords: Chemical reaction effect; magnetohydrodynamic (MHD); nanofluid; stagnation-point flow; stretching/shrinking sheet; suction/injection

ABSTRAK

Aliran titik genangan magnetohidrodinamik (MHD) nanobendalir terhadap permukaan telap meregang/mengecut dengan kesan tindak balas kimia dikaji. Persamaan menakluk dalam bentuk persamaan pembezaan separa tak linear dijelmakan kepada sistem persamaan pembezaan biasa tak linear menggunakan penjelmaan keserupaan seterusnya diselesaikan secara berangka menggunakan penyelesai masalah nilai sempadan, bvp4c dibina dalam perisian Matlab. Keputusan berangka diperoleh bagi pekali geseran kulit, nombor Nusselt setempat dan nombor Sherwood setempat serta profil halaju, suhu dan pecahan isi padu nanozarah bagi beberapa nilai parameter menakluk, iaitu parameter sedutan/semburan dan parameter tindak balas kimia. Penyelesaian dual didapati wujud bagi julat tertentu parameter regangan/kecutan. Analisis kestabilan dijalankan untuk menentukan penyelesaian yang stabil dan bermakna secara fizikal. Didapati bahawa penyelesaian pertama adalah stabil dan penyelesaian kedua tidak stabil.

Kata kunci: Aliran titik genangan; kesan tindak balas kimia; magnetohidrodinamik (MHD); nanobendalir; permukaan meregang/mengecut; sedutan/semburan

INTRODUCTION

The research of nanofluid has gained many attention in recent years. Choi (1995) was the first to introduce the word nanofluid that represents the fluid with nano scale particles whose diameter is less than 100 nm. Nanofluid is a new class of heat transfer fluids that comprise of a base fluid and nanoparticles. The use of additive is a technique applied to enhance the heat transfer performance of the base fluids (Noor et al. 2014). Due to small size and very large specific surface area of the nanoparticles, nanofluids have superior properties like thermal conductivity, minimal cloging in flow passages, long-term stability and homogeneity (Krishnamurthy et al. 2016). Thus, nanofluids have many applications in industry such as coolants, lubricants, heat exchangers, perstaltic pumps for diabetic treatements and nuclear applications. Therefore, quite many investigators have been studied the flow and thermal characteristics of

nanofluids, both theoretically and experimentally. It can be found in the papers by Arifin et al. (2011), Bachok et al. (2013), Hayat et al. (2016), Mansur and Ishak (2016), Mohamed et al. (2016), Othman et al. (2017) and Zaimi et al. (2017).

The study of heat and mass transfer problems with a chemical reaction have received a considerable amount of attention in recent years. This is due to the chemical reactions that can change the property and quality of any product (Shukla et al. 2017). Possible applications can be found in processes such as drying, energy transfer in a wet cooling tower, cooling of nuclear reactors, petroleum industries and flow in a desert cooler (Krishnamurthy et al. 2016; Venkateswarlu & Narayana 2015). Hence, many researchers have considered the effects of chemical reactions in different types of problems. Kameswaran et al. (2012) studied the hydromagnetic nanofluid due to a

stretching or shrinking sheet with viscous dissipation and chemical reaction effects. Besides that, Haile and Shankar (2015) investigated the boundary-layer flow of nanofluid over a moving surface in the presence of thermal radiation, viscous dissipation and chemical reaction effects. Other than that, the effects of Soret and heat source on steady MHD mixed convective heat and mass transfer flow past an infinite vertical plate embedded in a porous medium in the presence of chemical reaction, viscous and Joules dissipation was investigated by Ibrahim and Suneetha (2016). Recently, Gogoi (2015) considered the effects of chemical reaction on the flow over an exponentially stretching sheet. It is worth mentioning that Mishra and Singh (2017) reported the existence of dual solutions for the problem of forced convection flow over a stretching sheet with variable thickness in the presence of magnetic field.

In the present study, we examine numerically the MHD stagnation-point flow towards a vertical permeable stretching/shrinking sheet in a nanofluid with viscous dissipation and chemical reaction effects. This study is different from that considered by Othman et al. (2017), where we consider a horizontal stretching/shrinking sheet with the effects of magnetic field and chemical reaction are taken into consideration. Besides, a temporal stability analysis is performed to determine which solution is stable and has real physical implication. The effects of suction/injection, magnetic field and chemical reaction on the skin friction coefficient, local Nusselt number, local Sherwood number as well as velocity, temperature and concentration profiles are thoroughly examined and discussed.

MATHEMATICAL FORMULATION

We consider the steady two-dimensional stagnation-point flow of a nanofluid towards a permeable stretching/shrinking sheet, as shown in Figure 1. It is assumed that the velocity of the stretching/shrinking sheet is $u_w(x) = ax$, where $a > 0$ corresponds to the stretching sheet and $a < 0$ is for the shrinking case, while the free stream velocity is $u_e(x) = bx$, where b is a positive constant. Under these assumptions, the governing equations can be written as (Bachok et al. 2013; Othman et al. 2017; Raees et al. 2015):

$$\frac{\partial u}{\partial x} + \frac{\partial v}{\partial y} = 0 \tag{1}$$

$$u\frac{\partial u}{\partial x} + v\frac{\partial u}{\partial y} = u_e\frac{du_e}{dx} + v\frac{\partial^2 u}{\partial y^2} - \frac{\sigma B_0^2}{\rho_f}(u - u_e) \tag{2}$$

$$u\frac{\partial T}{\partial x} + v\frac{\partial T}{\partial y} = \alpha\frac{\partial^2 T}{\partial y^2} + \kappa\left[D_B\frac{\partial C}{\partial y}\frac{\partial T}{\partial y} + \left(\frac{D_T}{T_\infty}\right)\left(\frac{\partial T}{\partial y}\right)^2\right] \tag{3}$$

$$u\frac{\partial C}{\partial x} + v\frac{\partial C}{\partial y} = D_B\frac{\partial^2 C}{\partial y^2} + \left(\frac{D_T}{T_\infty}\right)\frac{\partial^2 T}{\partial y^2} - k_0(C - C_\infty) \tag{4}$$

where u and v are the velocity components in the x and y axes, respectively; v is the kinematic viscosity coefficient; B_0 is the imposed magnetic field; α is the thermal diffusivity of the base fluid; ρ_f is the density of the base fluid; T is the fluid temperature; T_w and C_w are, respectively, the temperature and the concentration at the surface, T_∞ and C_∞ are the ambient temperature and ambient concentration, respectively, $\kappa = (\rho c_p)_{np}/(\rho c_p)_f$ is the ratio of nanoparticles heat capacity to that of the base fluid heat capacity with c_p being the specific heat capacity at constant pressure; D_B is the Brownian diffusion coefficient; D_T is the thermophoresis diffusion coefficient; C is the fluid concentration and k_0 is the reaction rate parameter. We assume that (1)-(4) are subjected to the following boundary conditions:

$$u = u_w, v = v_w, T = T_w, C = C_w \text{ at } y = 0$$

$$u \rightarrow u_e, T \rightarrow T_\infty, C \rightarrow C_\infty \text{ as } y \rightarrow \infty \tag{5}$$

The following similarity variables for (1)-(5) are introduced:

$$\eta = (u_e/vx)^{1/2} y, \ \psi = (u_e vx)^{1/2} f(\eta),$$

$$\theta = (T - T_\infty)/(T_w - T_\infty), \phi = (C - C_\infty)/(C_w - C_\infty) \tag{6}$$

where ψ s the stream function defined as $u = \partial\psi/\partial y$ and $v = \partial\psi/\partial x$ which identically satisfies the continuity (1). By substituting (6) into (2) - (4), the following ordinary differential equations are obtained:

$$f''' + ff'' - f'^2 + 1 - M(f' - 1) = 0 \tag{7}$$

$$\frac{1}{\Pr}\theta'' + f\theta' + Nb\,\theta'\phi' + Nt\,\theta'^2 = 0 \tag{8}$$

$$\phi'' + Le(f\phi' - Cr\phi) + Sr\theta'' = 0 \tag{9}$$

and the boundary conditions (5) becomes,

$$f(0) = \gamma, f'(0) = \varepsilon, \theta(0) = 1, \phi(0) = 1,$$

$$f'(\eta) \rightarrow 1, \theta(\eta) \rightarrow 0, \phi(\eta) \rightarrow 0 \tag{10}$$

where prime denotes differentiation with respect to η,

$M = \dfrac{\sigma B_0^2}{\rho_f b}$, is the magnetic parameter with σ being the electrical conductivity; $\Pr = \dfrac{v}{\alpha}$ is the Prandtl number;

$Nb = \dfrac{\kappa D_B}{v}(C_w - C_\infty)$ is the Brownian motion parameter;

$Nt = \dfrac{\kappa D_T}{vT_\infty}(T_w - T_\infty)$ is the thermophoresis parameter; $Le = \dfrac{v}{D_B}$ is the Lewis number; $Cr = \dfrac{vk_0}{D_B b}$ is the chemical reaction

parameter; $Sr = \dfrac{D_T(T_w - T_\infty)}{D_B T_\infty(C_w - C_\infty)}$ is the Soret effect parameter,
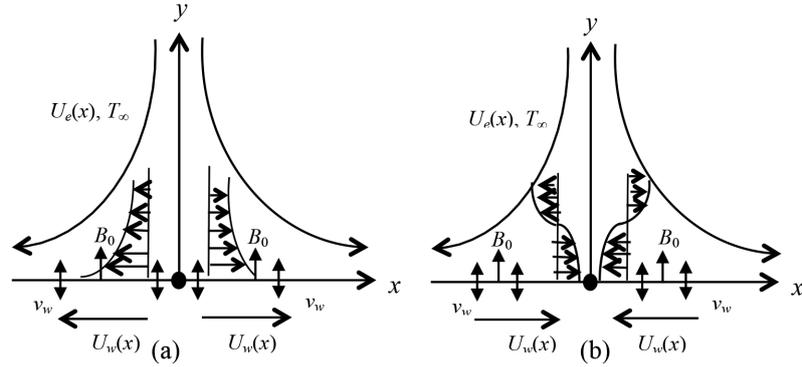
FIGURE 1. Physical model and coordinate system: (a) Stretching sheet and (b) Shrinking sheet

$\gamma = \dfrac{v_w}{-(bv)^{\frac{1}{2}}}$ is the suction/injection parameter and $\varepsilon = \dfrac{a}{b}$ is the stretching/shrinking parameter.

Quantities of physical interest in this problem are the skin friction coefficient, local Nusselt number and the local Sherwood number which are defined as (Othman et al. 2017),

$$C_f = \frac{\tau_w}{\rho_f u_e^2}, \; Nu_x = \frac{xq_w}{k(T_w - T_\infty)}, \; Sh_x = \frac{xq_m}{D_B(C_w - C_\infty)} \quad (11)$$

where τ_w is the surface shear stress; q_w is the surface heat flux; and q_m is the surface mass flux, which are given by Othman et al. (2017),

$$\tau_w = \mu\left(\frac{\partial u}{\partial y}\right)_{y=0}, \; q_w = -k\left(\frac{\partial T}{\partial y}\right)_{y=0}, \; q_m = -D_B\left(\frac{\partial C}{\partial y}\right)_{y=0} \quad (12)$$

where μ is the dynamic viscosity; and k is the thermal conductivity of nanofluids. By substituting (6) into (12) and using (11), the following expression can be attained,

$$\mathrm{Re}_x^{1/2}\, C_f = f''(0), \; \mathrm{Re}_x^{-1/2}\, Nu_x = -\theta'(0), \; \mathrm{Re}_x^{-1/2}\, Sh_x = -\phi'(0) \quad (13)$$

STABILITY OF SOLUTIONS

The idea of verifying the significance of dual solutions was started by Merkin (1985). Referring to Weidman et al. (2006), to study the temporal stability of the dual solutions, we need to study the unsteady state flow case. The governing equations (1) - (4) for the unsteady case are,

$$\frac{\partial u}{\partial x} + \frac{\partial v}{\partial y} = 0 \quad (14)$$

$$\frac{\partial u}{\partial t} + u\frac{\partial u}{\partial x} + v\frac{\partial u}{\partial y} = u_e\frac{du_e}{dx} + v\frac{\partial^2 u}{\partial y^2} - \frac{\sigma B_0^2}{\rho_f}(u - u_e) \quad (15)$$

$$\frac{\partial u}{\partial t} + u\frac{\partial T}{\partial x} + v\frac{\partial T}{\partial y} = \alpha\frac{\partial^2 T}{\partial y^2} + \kappa\left[D_B\frac{\partial C}{\partial y}\frac{\partial T}{\partial y} + \left(\frac{D_T}{T_\infty}\right)\left(\frac{\partial T}{\partial y}\right)^2\right] \quad (16)$$

$$\frac{\partial u}{\partial t} + u\frac{\partial C}{\partial x} + v\frac{\partial C}{\partial y} = D_B\frac{\partial^2 C}{\partial y^2} + \left(\frac{D_T}{T_\infty}\right)\frac{\partial^2 T}{\partial y^2} - k_0(C - C_\infty) \quad (17)$$

where t denotes the time. The new similarity transformation of the unsteady state problem by considering a dimensionless time variable τ is introduced as,

$$\eta = y\sqrt{\frac{b}{v}}, \; u = bx\frac{\partial f}{\partial \eta}(\eta,\tau), \; v = -(bv)^{\frac{1}{2}}f(\eta,\tau),$$

$$T = T_\infty + (T_w - T_\infty)\theta(\eta,\tau), \; C = C_\infty + (C_w - C_\infty)\phi(\eta,\tau), \; \tau = bt \quad (18)$$

Substituting (18) into (15)-(17), the following equations are obtained:

$$\frac{\partial^3 f}{\partial \eta^3} + f\frac{\partial^2 f}{\partial \eta^2} - \left(\frac{\partial f}{\partial \eta}\right)^2 + 1 - M\left(\frac{\partial f}{\partial \eta} - 1\right) - \frac{\partial^2 f}{\partial \eta \partial \tau} = 0 \quad (19)$$

$$\frac{1}{\mathrm{Pr}}\frac{\partial^2 \theta}{\partial \eta^2} + f\frac{\partial \theta}{\partial \eta} + Nb\frac{\partial \theta}{\partial \eta}\frac{\partial \phi}{\partial \eta} + Nt\left(\frac{\partial \theta}{\partial \eta}\right)^2 - \frac{\partial \theta}{\partial \tau} = 0 \quad (20)$$

$$\frac{\partial^2 \phi}{\partial \eta^2} + Le\left(f\frac{\partial \phi}{\partial \eta} - Cr\phi\right) + Sr\frac{\partial^2 \theta}{\partial \eta^2} - \frac{\partial \phi}{\partial \eta} = 0 \quad (21)$$

subject to the boundary conditions

$$f(0,\tau) = \gamma, \; \frac{\partial f}{\partial \eta}(0,\tau) = \varepsilon, \; \theta(0,\tau) = 1, \; \phi(0,\tau) = 1,$$

$$\frac{\partial f}{\partial \eta}(\eta,\tau) = 1, \; \theta(\eta,\tau) = 0, \; \phi(\eta,\tau) = 0, \text{ as } \eta \to \infty \quad (22)$$

In order to test the stability behavior, the basic flow $f = f_0(\eta)$, $\theta = \theta_0(\eta)$ and $\phi = \phi_0(\eta)$ which is obtained from (19)-(21) will be perturbed with disturbance (Weidman et al. 2006)

$$f(\eta,\tau) = f_0(\eta) + e^{-\lambda\tau} F(\eta),$$

$$\theta(\eta,\tau) = \theta_0(\eta) + e^{-\lambda\tau} G(\eta), \qquad (23)$$

$$\phi(\eta,\tau) = \phi_0(\eta) + e^{-\lambda\tau} H(\eta)$$

where λ is an unknown eigenvalue, and $F(\eta)$, $G(\eta)$ and $H(\eta)$ are small relative to $f_0(\eta)$, $\theta_0(\eta)$ and $\phi_0(\eta)$. Solutions of the eigenvalue problem (19)-(22) give an infinite set of eigenvalues $\lambda_1 < \lambda_2 < \lambda_3 \dots$, if λ_1 is negative, there is an initial growth of disturbances and the flow is unstable but when λ_1 is positive, there in an initial decay and the flow is stable. By substituting (23) into (19)-(21), one obtains the following linearized problem:

$$F''' + f_0 F'' - \left(2f_0' + M - \lambda\right)F' + f_0'' F_0 = 0 \qquad (24)$$

$$\frac{1}{\Pr}G'' + \left(f_0 + Nb\phi_0 + 2Nt\theta'\right)G' + \lambda G + \theta_0' F + Nb\theta_0' H' = 0 \qquad (25)$$

$$H'' + Le f_0 H' - \left(Le\,Cr + \lambda\right)H + Le\,\phi_0' F + Sr\,G'' = 0 \qquad (26)$$

subject to the boundary conditions,

$$F(0) = 0,\ F'(0) = 0,\ G(0) = 0,\ H(0) = 0,$$

$$F'(\eta) \to 0,\ G(\eta) \to 0,\ H(\eta) \to 0 \ \text{as}\ \eta \to \infty \qquad (27)$$

The boundary conditions (27) are obtained by substituting (23) into the boundary conditions (22) and using the boundary conditions (10), for the steady state solutions.

RESULTS AND DISCUSSION

The ordinary differential equations (7)-(9) subject to the boundary conditions (10) were solved numerically using the bvp4c function in Matlab software. The results obtained illustrate the effects of some governing parameters on the skin friction coefficient, $\mathrm{Re}_x^{-1/2} C_f$, the local Nusselt number (represents the heat transfer rate), $\mathrm{Re}_x^{-1/2} Nu_x$ and local Sherwood number (represents the mass transfer rate), $\mathrm{Re}_x^{-1/2} Sh_x$, as well as velocity profile $f'(\eta)$, temperature profile $\theta(\eta)$ and concentration profile $\phi(\eta)$. Effects of the suction/injection parameter γ and chemical reaction parameter Cr on the flow and heat transfer characteristics are thoroughly examined and discussed.

In order to validate the present numerical results, we compare our results with those reported by Othman et al. (2017) for the case when the buoyancy effect is absent, i.e. $\lambda = 0$ and $N_r = 0$ in (7) of that paper. The comparisons are found to be in a very good agreement as shown in Table 1, therefore, gives confidence to the numerical results that will be reported further. On the other hand, the values of $\mathrm{Re}_x^{-1/2} C_f$, $\mathrm{Re}_x^{-1/2} Nu_x$ and $\mathrm{Re}_x^{-1/2} Sh_x$ for different values of γ are tabulated in Table 2. From Table 2, it is clearly shown that the values of $|\mathrm{Re}_x^{-1/2} C_f|$, $|\mathrm{Re}_x^{-1/2} Nu_x|$ and $|\mathrm{Re}_x^{-1/2} Sh_x|$ increase as the suction/injection parameter γ increases.

Figures 2-4 show the variation of the skin friction coefficient, local Nusselt number and local Sherwood number with stretching/shrinking parameter ε for different values of suction/injection parameter γ. From Figures 2-4, it is found that it is possible to obtain dual solutions of the similarity equations (7)-(9) subject to the boundary conditions (10). Numerical solutions exist in three different range of stretching/shrinking parameter ε as depicted in Figures 2-4. There exist a critical value of ε denoted by ε_c in the shrinking region, with dual solutions exist for $\varepsilon > \varepsilon_c$, a unique solution found when $\varepsilon = \varepsilon_c$ and no solution obtained for $\varepsilon < \varepsilon_c$. Based on our computation, the critical values ε_c obtained are $\varepsilon_{c1} = -1.21168$, $\varepsilon_{c2} = -1.25537$ and $\varepsilon_{c2} = -1.30290$ for $\gamma = -0.1$, 0 and 0.1, respectively, as shown in Figures 2-4.

In the following discussion, we categorize the first and second solutions by how they appear in Figure 2, i.e. the first solution has a higher value of $\mathrm{Re}_x^{-1/2} C_f$ than the second solution for a given ε. From Figure 2, we can see that as γ increases, the skin friction coefficient increases. This is due to the suction effect that increasing the surface shear stress, delay the fluid flow and thus, increase the velocity gradient at the surface which is consistent with the graph in Figure 6. Figure 2 also indicate that the critical values stretching/shrinking parameter ε_c for which the solution

TABLE 1. Comparison for the values of $\mathrm{Re}_x^{-1/2} C_f$, $\mathrm{Re}_x^{-1/2} Nu_x$ and $\mathrm{Re}_x^{-1/2} Sh_x$ for different values of ε, taking $\lambda = 0$ and $N_r = 0$ in (7) of Othman et al. (2017) by setting $f(0) = 0$ in boundary condition (10) with $\Pr = 7$, $M = Cr = 0$, $Nb = Nt = 0.1$ and $Le = Sr = 1$

ε	Othman et al. (2017)			Present results		
	$\mathrm{Re}_x^{-1/2} C_f$	$\mathrm{Re}_x^{-1/2} Nu_x$	$\mathrm{Re}_x^{-1/2} Sh_x$	$\mathrm{Re}_x^{-1/2} C_f$	$\mathrm{Re}_x^{-1/2} Nu_x$	$\mathrm{Re}_x^{-1/2} Sh_x$
-1.0	1.328817	0.016105	0.440494	1.328817	0.016105	0.440494
-0.5				1.495670	0.347080	0.455138
0				1.232588	0.810030	0.206842
0.5				0.713295	1.211774	-0.019361
1.0				0	1.551483	-0.204060

TABLE 2. Values of $\mathrm{Re}_x^{-1/2}\,C_f$, $\mathrm{Re}_x^{-1/2}\,Nu_x$ and $\mathrm{Re}_x^{-1/2}\,Sh_x$ when $\mathrm{Pr} = 7$, $Nb = Nt = 0.1$, $\varepsilon = 1.2$, $M = 0.01$, $Cr = 0.1$ and $Le = Sr = 1$

γ	$\mathrm{Re}_x^{-1/2}\,C_f$		$\mathrm{Re}_x^{-1/2}\,Nu_x$		$\mathrm{Re}_x^{-1/2}\,Sh_x$	
	First solution	Second solution	First solution	Second solution	First solution	Second solution
-0.10	0.681315	0.338875	0	0	0.183503	0.120101
-0.05	0.840219	0.258870	0.000005	0	0.244333	0.118185
0	0.969009	0.209455	0.000084	0	0.307754	0.119658
0.05	1.085936	0.172333	0.000650	0	0.374956	0.122316
0.10	1.196428	0.142025	0.003306	0	0.444150	0.125640
0.15	1.302943	0.116021	0.012476	0	0.509990	0.129436
0.20	1.406822	0.092927	0.037364	0	0.561448	0.133623
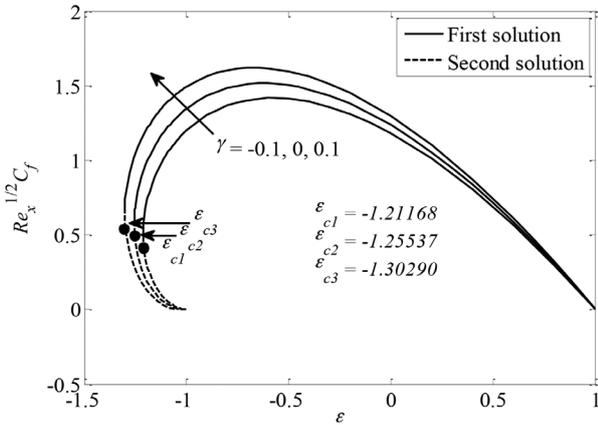
FIGURE 2. Variation of the skin friction coefficient $\mathrm{Re}_x^{-1/2}\,C_f$ with ε for different values of γ when $M = 0.01$
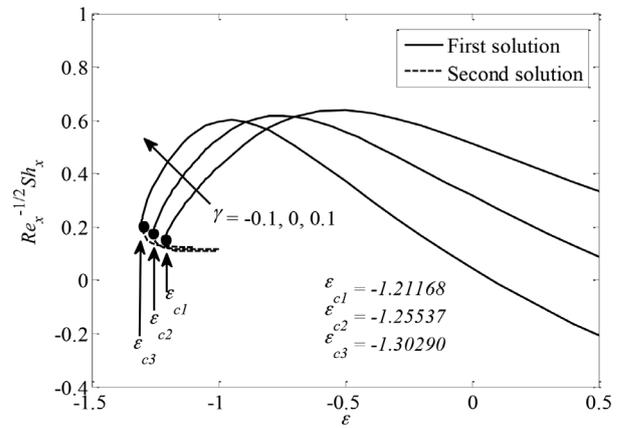
FIGURE 4. Variation of the local Sherwood number $\mathrm{Re}_x^{-1/2}\,Sh_x$ with ε for different values of γ when $\mathrm{Pr} = 7$, $M = 0.01$, $Nb = 0.1$. $Nt = 0.1$, $Le = 1$, $Cr = 0.1$ and $Sr = 1$
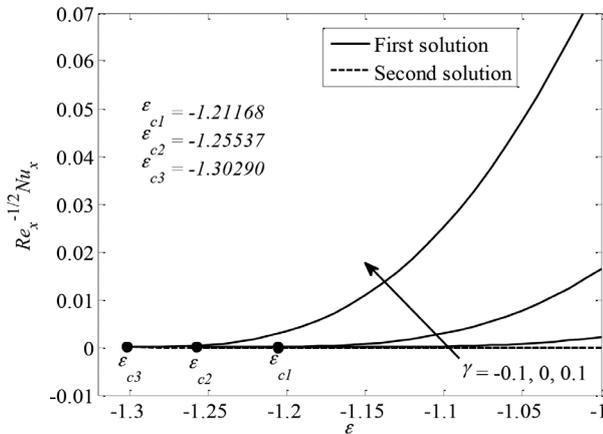
FIGURE 3. Variation of the local Nusselt number $\mathrm{Re}_x^{-1/2}\,Nu_x$ with ε for different values of γ when $\mathrm{Pr} = 7$, $M = 0.01$, $Nb = 0.1$, $Nt = 0.1$, $Le = 1$, $Cr = 0.1$ and $Sr = 1$
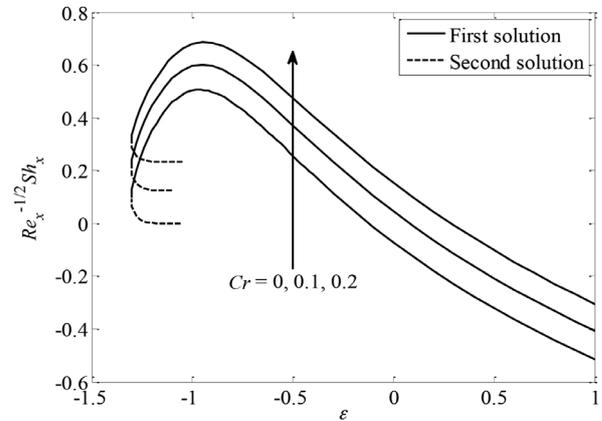
FIGURE 5. Variation of the local Sherwood number $\mathrm{Re}_x^{-1/2}\,Sh_x$ with ε for different values of Cr when $\mathrm{Pr} = 7$, $M = 0.01$, $Nb = 0.1$, $Nt = 0.1$, $Le = 1$, $\gamma = 0.1$ and $Sr = 1$
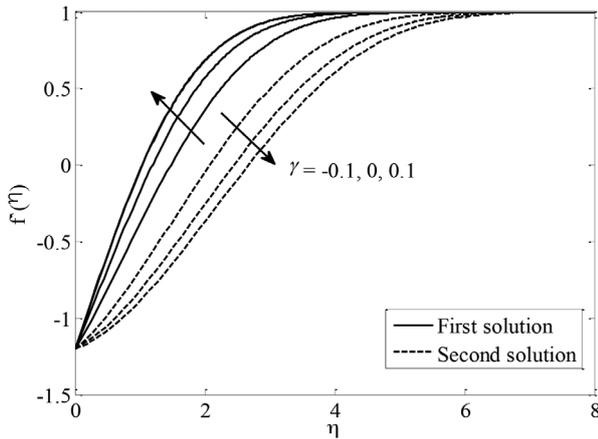
FIGURE 6. The velocity profiles $f'(\eta)$ for different values of γ when $M = 0.001$ and $\varepsilon = 1.2$ (shrinking case)
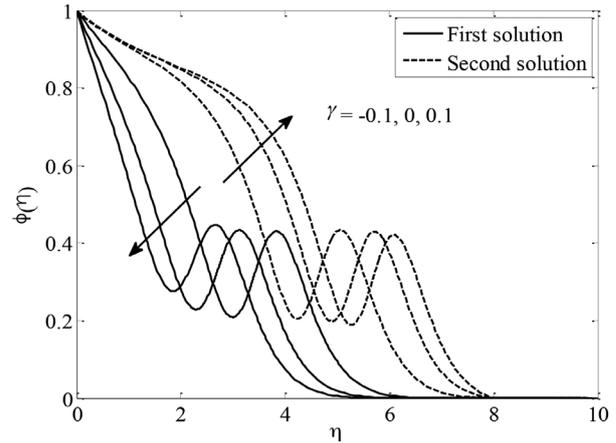

FIGURE 8. The concentration profiles $\phi(\eta)$ for different values of γ when $Pr = 7$, $M = 0.01$, $Nb = 0.1$, $Nt = 0.1$, $Le = 1$, $Cr = 0.1$, $Sr = 1$ and $\varepsilon = 1.2$ (shrinking case)
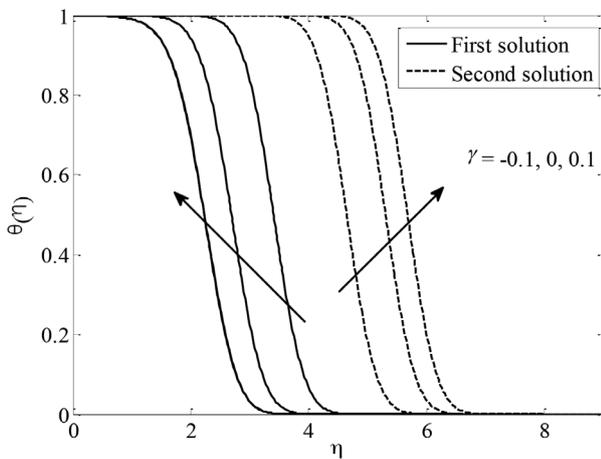

FIGURE 7. The temperature profiles $\theta(\eta)$ for different values of γ when $Pr = 7$, $M = 0.01$, $Nb = 0.1$, $Nt = 0.1$, $Le = 1$, $Cr = 0.1$, $Sr = 1$ and $\varepsilon = 1.2$ (shrinking case)
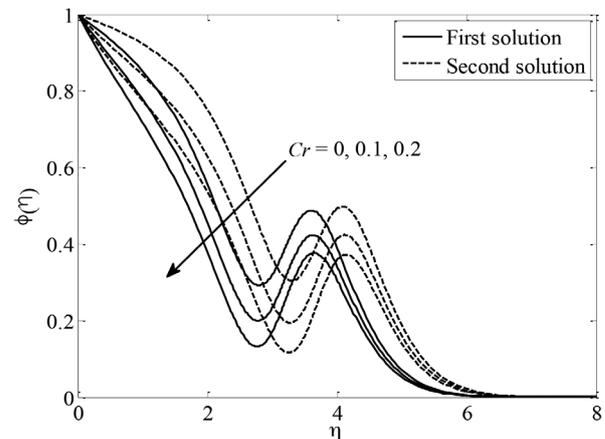

FIGURE 9. The concentration profiles $\phi(\eta)$ for different values of Cr when $Pr = 7$, $M = 0.01$, $Nb = 0.1$, $Nt = 0.1$, $Le = 1$, $\gamma = 0.1$, $Sr = 1$ and $\varepsilon = 1.3$ (shrinking case)

exist increase as γ increases, suggests that suction widens the region of dual solutions to the similarity equations (7)-(10).

Figure 3 shows the magnitude of the local Nusselt number $\left| Re_x^{-1/2} Nu_x \right|$ which represents the heat transfer rate at the surface increases when the suction parameter γ increases. It is because the fact that increasing γ decreases the thermal boundary layer thickness for the first solutions and in turn increases the temperature gradient at the surface. In Figure 4, it is seen that the values of $Re_x^{-1/2} Sh_x$ which represents the mass transfer rate at the surface increases as γ increases. It is found that the first solution has a higher values of $Re_x^{-1/2} Sh_x$ than the second solution for a given ε.

The variation of the local Sherwood number $Re_x^{-1/2} Sh_x$ with ε for some values of the chemical reaction parameter Cr is shown in Figure 5. It is noted that the mass transfer rate at the surface increases with increasing of Cr as depicted in Figure 5. This is because imposing chemical

reaction effect decreases the concentration boundary layer thickness and thus increasing the concentration gradient. As a result, the mass transfer rate at the surface increases.

Figures 6-8 demonstrate the effects of suction/injection parameter γ on $f'(\eta)$, $\theta(\eta)$ and $\phi(\eta)$ representing velocity, temperature and concentration profiles, respectively. As apparent in Figure 6, it is seen that the velocity increases as γ increases for the first solution. This phenomenon occurs due to suction effect cause the reduction of momentum boundary layer thickness and thus increases the flow near the surface. The opposite behaviours are observed for the second solution as depicted in Figure 6 where velocity of the fluid decreases with an increase in γ. This is due to suction effect which retards the fluid motion. Figure 7 shows that the temperature gradient $\theta'(0) \approx 0$ for all values of γ considered, which is consistent with the local Nusselt number presented in Figure 3.

Figures 8 and 9 show the concentration profiles for different values of suction/injection parameter γ and

TABLE 3. Smallest eigenvalue, λ_1 for some values of ε when $M = 0.01$, Pr = 7, $Cr = 0.1$, $Le = Sr = 1$ and $Nb = Nt = \gamma = 0.1$

ε	First solution (Upper branch)	Second solution (Lower branch)
-1.1	1.2508	-0.9726
-1.15	1.0806	-0.8775
-1.2	0.8803	-0.7472
-1.25	0.6240	-0.5572
-1.3	0.1417	-0.1381
-1.302	0.0786	-0.0775
-1.30289	0.0089	-0.0089
-1.3029	0.0000	-0.0034

chemical reaction parameter Cr, respectively. Different from the velocity and the temperature profiles presented in Figures 6 and 7 which show monotonically increasing or decreasing, the concentration profiles show a fluctuate trend near the surface $\eta = 0$ before asymptotically reach the far field boundary condition $\phi(\eta) \rightarrow 0$ as $\eta \rightarrow \infty$, which supports the validity of the numerical results. Similar results were reported by Othman et al. (2017). Figure 8 also shows that the boundary layer thickness for the concentration profiles decreases with increasing values of γ, for both first and second solutions, inconsequence increases the concentration gradient at the surface. This phenomenon causes the mass transfer rate at the surface to increase with increasing γ, which is consistent with the results shown in Figure 4.

Figure 9 shows the influences of chemical reaction parameter Cr on the concentration profile. It is found that the concentration of both solutions decrease as Cr increases. It can be seen that a significant reduction in the concentration boundary layer thickness in both solutions as Cr is increased. This leads to increase in concentration gradient and in turn increase the mass transfer rate at the surface which is consistent with the results illustrated in Figure 5. It is worth highlighting that in all Figures 6 to 9 illustrate here, the velocity, temperature and concentration profiles satisfy the far field boundary conditions (10) asymptotically, which support the validity of the numerical results and the existence of the dual solutions obtained.

As been discussed before, the dual solutions exist for a certain range of the shrinking strength. Hence, a temporal stability analysis is carried out to verify which solution could be utilized in the real world phenomena. A stability analysis is carried out by solving linear eigenvalue problem (24-26) subject to the boundary conditions (27). The stable solutions are identified based on the positive smallest eigenvalues λ in the relations $f(\eta, \tau) = f_0(\eta) + e^{-\lambda\tau}F(\eta)$, $\theta(\eta, \tau) = \theta_0(\eta) + e^{-\lambda\tau}G(\eta)$ and $\phi(\eta, \tau) = \phi_0(\eta) + e^{-\lambda\tau}H(\eta)$ given in (23), whereas the unstable solution is recognized based on the negative smallest eigenvalues λ. As the time pass, $\tau \rightarrow \infty$, positive values of λ give an initial decay of disturbance which results in a stable flow, whereas negative values of λ results in the growth of disturbance and causes an unstable flow. Table 3 shows that the values of λ are positive for the first solution, thus the first solutions are stable and physically reliable while the second solutions are not.

CONCLUSION

We have examined numerically the problem of steady two-dimensional stagnation-point flow of a nanofluid toward a permeable stretching/shrinking sheet. From this study, the skin friction coefficient, the local Nusselt number and the local Sherwood number increased as the suction/injection parameter is increased. The local Sherwood number was found to decrease when the chemical reaction effect is imposed. Dual solutions were found to exist for a certain range of the shrinking strength but for the stretching case, unique solution was found. A temporal stability analysis was performed to prove that the first solution (upper branch) is stable, while the second solution (lower branch) is unstable.

REFERENCES

Arifin, N.M., Nazar, R. & Pop, I. 2011. Viscous flow due to a permeable stretching/shrinking sheet in a nanofluid. *Sains Malaysiana* 40(12): 1359-1367.

Bachok, N., Ishak, A. & Pop, I. 2013. Boundary layer stagnation-point flow toward a stretching/shrinking sheet in a nanofluid. *Journal of Heat Transfer* 135: 1-5.

Choi, S.U.S. & Eastman, J.A. 1995. *Enhancing Thermal Conductivity of Fluids with Nanoparticles*. doi:. https://www.osti.gov/servlets/purl/196525.

250

Gogoi, M.K. 2015. Effects of chemical reaction on MHD boundary layer flow over an exponentially stretching sheet with Joule heating and thermal radiation. *International Research Journal of Engineering and Technology* 2: 768-773.

Haile, E. & Shankar, B. 2015. Boundary-layer flow of nanofluids over a moving surface in the presence of thermal radiation, viscous dissipation and chemical reaction. *Applications and Applied Mathematics: An International Journal* 10(2): 952-969.

Hayat, T., Aziz, A., Muhammad, T. & Alsaedi, A. 2016. On magnetohydrodynamic three-dimensional flow of nanofluid over a convectively heated nonlinear stretching surface. *International Journal of Heat and Mass Transfer* 100: 566-572.

Ibrahim, S.M. & Suneetha, K. 2016. Heat source and chemical effects on MHD convection flow embedded in a porous medium with Soret, viscous and Joules dissipation. *Ain Shams Engineering Journal* 7(2): 811-818.

Kameswaran, P.K., Narayana, M., Sibanda, P. & Murthy, P.V.S.N. 2012. Hydromagnetic nanofluid flow due to a stretching or shrinking sheet with viscous dissipation and chemical reaction effects. *International Journal of Heat and Mass Transfer* 55: 7587-7595.

Krishnamurthy, M.R., Prasannakumara, B.C., Gireesha, B.J. & Gorla, R.S.R.G. 2016. Effect of chemical reaction on MHD boundary layer flow and melting heat transfer of Williamson nanofluid in porous medium. *Engineering Science and Technology, An International Journal* 19(1): 53-61.

Mansur, S. & Ishak, A. 2016. Unsteady boundary layer flow of a nanofluid over a stretching/shrinking sheet with a convective boundary condition. *Journal of the Egyption Mathematical Society* 24(4): 650-655.

Merkin, J.H. 1985. On dual solutions occurring in mixed convection in a porous medium. *Journal of Engineering Mathematics* 20(2): 171-179.

Mishra, U. & Singh, G. 2017. Dual solutions of forced convection flow along a stretching sheet with variable thickness in presence of free stream and magnetic field. *Sains Malaysiana* 46(2): 349-358.

Mohamed, M.K.A., Noar, N.A.Z.M., Salleh, M.Z. & Ishak, A. 2016. Free convection boundary layer flow on a horizontal circular cylinder in a nanofluid with viscous dissipation. *Sains Malaysiana* 45(2): 289-296.

Noor, A., Nazar, R. & Jafar, K. 2014. Stability analysis of stagnation-point flow past a shrinking sheet in a nanofluid. *Journal of Quality Measurement and Analysis* 10(2): 51-63.

Othman, N.A., Yacob, N.A., Bachok, N., Ishak, A. & Pop, I. 2017. Mixed convection boundary-layer stagnation point flow past a vertical stretching/shrinking surface in a nanofluid. *Applied Thermal Engineering* 115: 1412-1417.

Raees, A., Xu, H., Sun, Q. & Pop, I. 2015. Mixed convection in gravity-driven nano-liquid film containing both nanoparticles and gyrotactic microorganisms. *Applied Mathematics and Mechanics (English Edition)* 36(2): 163-178.

Shukla, N., Rana, P., Beg, O.A. & Singh, B. 2017. Effect of chemical reaction and viscous dissipation on MHD nanofluid flow over a horizontal cylinder: Analytical solution. *AIP Conference Proceeding* 1802: 20015.

Venkateswarlu, B. & Narayana, P.S. 2015. Chemical reaction and radiation absorption effects on the flow and heat transfer of a nanofluid in a rotating system. *Applied Nanoscience* 5(3): 351-360.

Weidman, P.D., Kubitschek, D.G. & Davis, A.M.J. 2006. The effect of transpiration on self- similar boundary layer flow over moving. *International Journal of Engineering Science* 44(11-12): 730-737.

Zaimi, K., Ishak, A. & Pop, I. 2017. Unsteady flow of a nanofluid past a permeable shrinking cylinder using Buongiorno's model. *Sains Malaysiana* 46(9): 1667-1674.

Fatinnabila Kamal & Khairy Zaimi
Institut Matematik Kejuruteraan
Universiti Malaysia Perlis
02600 Arau, Perlis Indera Kayangan
Malaysia

Anuar Mohd Ishak*
Pusat Pengajian Sains Matematik
Fakulti Sains dan Teknologi
Universiti Kebangsaan Malaysia
43600 UKM Bangi, Selangor Darul Ehsan
Malaysia

Ioan Pop
Department of Mathematics
Babeş-Bolyai University
400084 Cluj-Napoca
Romania

*Corresponding author; email: anuar_mi@ukm.edu.my